Journal of Colloid and Interface Science 350 (2010) 290–294

Contents lists available at ScienceDirect

Journal of Colloid and Interface Science

www.elsevier.com/locate/jcis

Hierarchical structured ZSM-5 zeolite of oriented nanorods and its performance in the alkylation of phenol with isopropanol

Deju Wang [a,b], Xueli Li [b], Zhongneng Liu [b], Yahong Zhang [a], Zaiku Xie [b], Yi Tang [a,*]

[a] Department of Chemistry, Shanghai Key Laboratory of Molecular Catalysis and Innovative Materials and Laboratory of Advanced Materials, Fudan University, Shanghai 200433, People's Republic of China
[b] Shanghai Research Institute of Petrochemical Technology, SINOPEC, Shanghai 201208, People's Republic of China

ARTICLE INFO

Article history:
Received 3 March 2010
Accepted 19 May 2010
Available online 23 May 2010

Keywords:
Hierarchical ZSM-5 zeolite
Nanorods
Alkylation
Phenol
Isopropanol

ABSTRACT

Hierarchical structured ZSM-5 zeolite of *c*-axis-oriented nanorods has been prepared by a zeolite-seed-assisted hydrothermal synthesis method without any type of mesoscale template. The final product has loose aggregation which consists of rod-like nanocrystals with widths of about 20–30 nm, formed by the oriented aggregation model. The nitrogen physisorption suggested that the hierarchical structured ZSM-5 zeolite had higher mesopore volume and external surface area than the sample prepared conventionally. Due to the shortened microporous channel and opening mesopore, the prepared HZSM-5 catalyst presents high catalytic activity and stability for the alkylation of phenol with isopropanol.

1. Introduction

Zeolites are widely used in areas of catalysis, separation, ion exchange, and sensing because of their uniform pore size, high surface area, and good thermal stability [1–4]. Recently, a growing interest in this field is focusing on the preparation of zeolites with short diffusion paths and/or hierarchical porosities to meet the specific demands in bulky molecule-involved and/or diffusion-controlled catalytic reactions [5–21]. Supermicro- or mesopores containing zeolites represent the typical structure of such materials, which are generally fabricated by extracting the framework elements or through a mesoscale template technique [8–21]. Dealumination or desilication methods have been well developed for the generation of intracrystal secondary pores in the past decades, but they are generally limited by the partial damage of the framework and the blockage of the micropores by the extraframework residue generated during the hydrothermal treatment and chemical extraction [8–11]. The mesopores could also be created within the zeolite crystals through assembly of zeolite nanocrystals on the mesoscale templates in a versatile manner, such as using rigid templates of nanosized or mesoporous carbon [12–16] and using soft templates of organosilane surfactant or cationic polymers [17–21]. However, the mesoscale template pathway is rather complicated and less facile.

Herein, a mesoscale template-free route is demonstrated for the synthesis of hierarchical structured ZSM-5 zeolite of *c*-axis-oriented nanorods using a zeolite-seed-assisted hydrothermal synthesis method. Due to a unique intersecting channel system in the ZSM-5 framework with a straight 10-member ring (10MR) channel parallel to the *b*-axis and a zig–zag 10MR channel extending along the *a*-axis [22–25], the prepared hierarchical ZSM-5 zeolite of *c*-axis-oriented nanorods is very important for their enriched exposed pore opening and shortened channels.

2. Materials and methods

Silicalite-1 seeds were prepared according to a previous report [26]. Typically, a gel with the composition of molar ratio of $6Na_2O{:}0.83Al_2O_3{:}100SiO_2{:}1500H_2O$ was then prepared using NaOH, $Al_2(SO_4)_3{\cdot}18H_2O$, silica sol with 40% SiO_2 content, and distilled water as the raw materials. Afterward, 5 g of prepared silicalite-1 seed sol and 1 g of 1,6-hexylenediamine were added in 100 g of the above gel with vigorous stirring. Then, the mixture was enclosed in a PTFE-lined stainless-steel autoclave and heated at 160 °C for different time intervals from 2 to 24 h. The products were denoted as NZ160-*X*, in which *X* means the crystallization time (h). By hydrothermal treating the gel with the same composition as above but without seeds, the reference samples of CZ-1 and CZ-2 were synthesized at 160 °C for 3 and 5 days, respectively; CZ-3 was also obtained without seeds but with a double dosage of 1,6-hexylenediamine after crystallization at 160 °C for 5 days. All the resulting products were washed intensively with distilled

* Corresponding author. Fax: +86 21 65641740.
E-mail addresses: djwang@sript.com.cn (D. Wang), yitang@fudan.edu.cn (Y. Tang).

0021-9797/$ - see front matter © 2010 Elsevier Inc. All rights reserved.
doi:10.1016/j.jcis.2010.05.065

water and finally dried at 110 °C, followed by calcination at 550 °C to remove the organic template. The protonated form of the samples was obtained by ion exchange with NH_4NO_3 solution, followed by calcination at 500 °C for 4 h.

3. Results and discussion

The reference samples prepared without seeding are characterized first. The low X-ray diffraction (XRD) peaks of CZ-1 demonstrate its relative low crystallinity despite hydrothermal treatment for 3 days (Fig. 1A-a) and the small particles matching with amorphorous materials are obviously observed in its scanning electron microscopy (SEM) image (Fig. 1B). When prolonging the crystallization time to 5 days, the crystallinity of CZ-2 is obviously enhanced (Fig. 1A-b), but some small amorphorous materials are still identified in its SEM image (Fig. 1C). To obtain ZSM-5 zeolite with complete crystallization, a double amount of 1,6-hexylenediamine must be adopted. In this case, the large ZSM-5 crystals (CZ-3) can be obtained after crystallization for 5 days (Fig. 1A-c and D), which is selected as the micrometer-sized reference sample below.

Fig. 2 shows the SEM images of the NZ160-*X* samples synthesized with silicalite-1 seeds at different time intervals. The small irregular granules are observed in NZ160-02 (Fig. 2A), while the particles with sizes of 200–300 nm are obtained after crystallization for 4 h (Fig. 2B), and their size changes little with prolonging of the crystallization time (Fig. 2C and D). Additionally, it is also found that the surfaces of the NZ160-08 and NZ160-24 particles are very rough (Fig. 2C and D), probably indicating that they are composed of tiny granules of very small size. The XRD patterns of the NZ160-*X* samples are displayed in Fig. 3A. A negligible amount of the ZSM-5 phase could be identified in the XRD pattern of NZ160-02 (Fig. 3A-a), indicating that the sample obtained at this stage is still mainly amorphous materials. However, in NZ160-04, the characteristic diffraction peaks of ZSM-5 zeolite are clearly observed (Fig. 3A-b), and the broad dispersed peak at 20–30° belonging to the amorphous phase almost disappears. The crystallinity of the products reaches a maximum with the crystallization time being prolonged to 8 h (Fig. 3A-c) and is no longer increased with the proceeding of crystallization (Fig. 3A-d). The relative broad XRD peaks might reflect that the NZ160-*X* products are composed of nanosized zeolite crystals, compared with their micrometer-sized counterpart (Fig. 1A). These imply that the preadded silicalite-1 seeds could effectively accelerate the crystallization of ZSM-5 zeolite and decrease the crystal size.

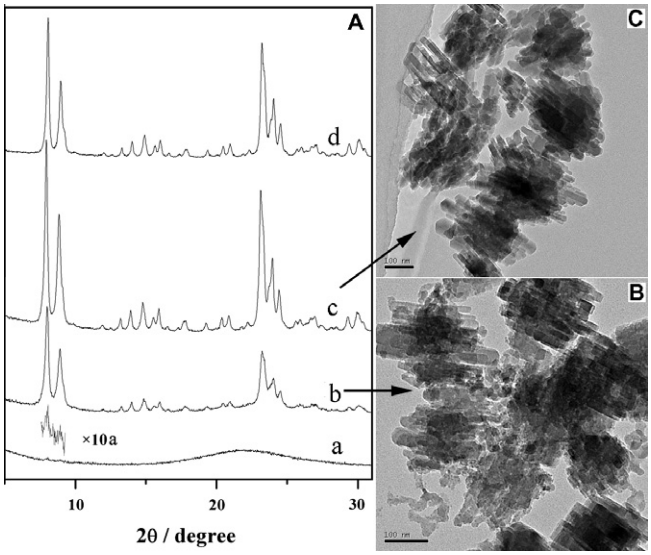

Fig. 3. XRD patterns: (A) of (a) NZ160-02, (b) NZ160-04, (c) NZ160-08, and (d) NZ160-24; and TEM images of (B) NZ160-04 and (C) NZ160-08. The scale bars in (B and C) are 100 nm.

The fine structures of the as-synthesized NZ160-*X* samples are further investigated by transmission electron microscopy (TEM) experiments. Small spheres with sizes of about 30 nm are clearly

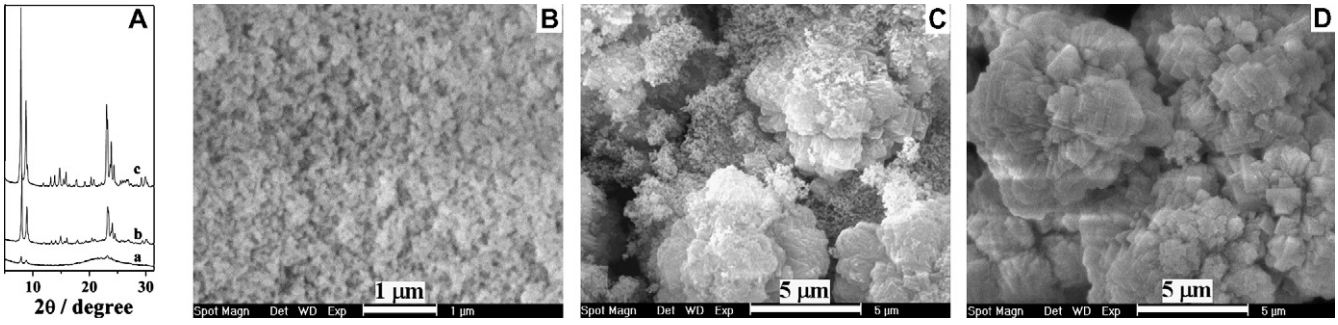

Fig. 1. XRD patterns: (A) of (a) CZ-1, (b) CZ-2, and (c) CZ-3; and SEM images of (B) CZ-1, (C) CZ-2 and (D) CZ-3.

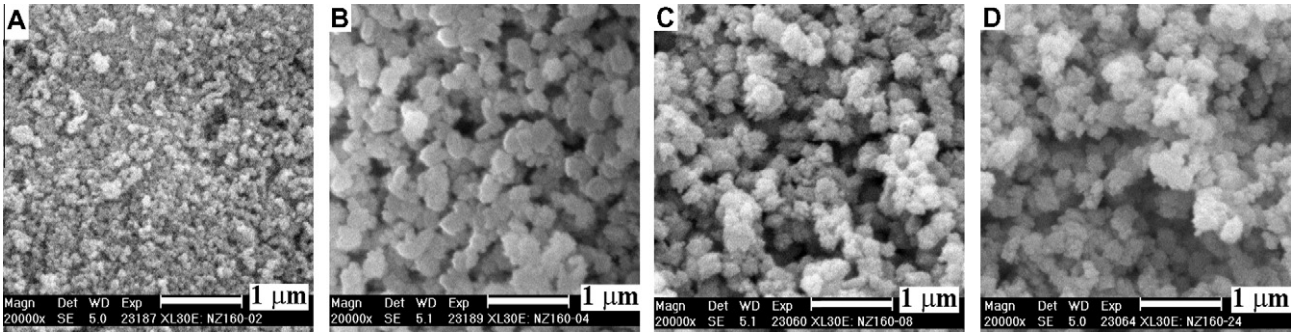

Fig. 2. SEM images of: (A) NZ160-02, (B) NZ160-04, (C) NZ160-08, and (D) NZ160-24.

observed within NZ160-02 (Fig. 4), which are mostly attributed to the amorphous phase, referring to the XRD pattern (Fig. 3A-a). Moreover, a few crystalline domains with sizes below 60 nm are also observed embedded among these spheres (Fig. 4A), and some of the very small crystalline domains in the particles might come from the secondary nucleation. Additionally, the crystallite aggregates with almost the same crystal lattice fringes contained in NZ160-02 are likely derived from the preadded silicalite-1 seeds (Fig. 4B). After crystallization for 4 h, the aluminosilicate gel has transformed into agglomerates of rod-like ZSM-5 nanocrystals (Fig. 3B) with the shape and size almost the same as those of the product crystallized for a long time (Fig. 3C), but their XRD peaks (Fig. 3A-b) are much weaker than those of the latter (Fig. 3A-c). It might imply that some of the particles are not well crystallized at this stage. When the crystallization time is prolonged to 8 h, all the products exist as agglomerates of the well-crystallized ZSM-5 nanorods with widths of 20–30 nm (Fig. 5A and B), and their XRD peaks reach a maximum as shown in Fig. 1A-c. It is also found that after crystallization for 4 h, all products possess enriched opening mesopores within the product particles from the low-contrast regions among the intergrown rod-like nanocrystals (Fig. 3B and C). It is remarkable that the TEM images of NZ160-08 (Fig. 5A) show that the crystal lattice fringes significantly spread throughout the entire particle despite the existence of many mesopores, and the selected-area electron diffraction (SAED) pattern (Fig. 5C) taken from Fig. 5B clearly presents a set of well-indexed diffraction points of ZSM-5 zeolite. These facts evidently proved that the final product has a nanometer-scale polycrystalline architecture of highly *c*-axis-oriented ZSM-5 zeolite nanorods with tens of nanometers in width, like a monocrystal. For the short channels of ZSM-5 nanorods and the opening mesopores among the oriented nanorods, such material is capable of enhancement of the diffusion properties in the catalytic reaction.

The textural properties of samples are listed in the Table 1. It is found that both the surface area (S_{Micro}) and pore volume (V_{Micro}) of the micropore increase with prolonging of the crystallization time for NZ160-*X*, indicating the enhancement of the crystallinity of the samples. In contrast, the mesopore volume (V_{Meso}) presents a monotonous decline but the external surface area (S_{Ext})

Table 1
Textural properties of the samples.

Samples	S_{BET} ($m^2\ g^{-1}$)	S_{Micro} ($m^2\ g^{-1}$)	S_{Ext}[a] ($m^2\ g^{-1}$)	V_{Micro}[a] ($cm^3\ g^{-1}$)	V_{Meso}[a] ($cm^3\ g^{-1}$)
NZ160-02	86.14	12.2	73.9	0.005	0.241
NZ160-04	252.2	169.2	83.0	0.083	0.184
NZ160-08	369.6	246.2	123.4	0.122	0.173
NZ160-24	366.0	251.1	114.9	0.124	0.143
CZ-3	313.4	247.8	65.6	0.122	0.048

[a] Determined by *t* plot according to the method of Lepens and de Boer.

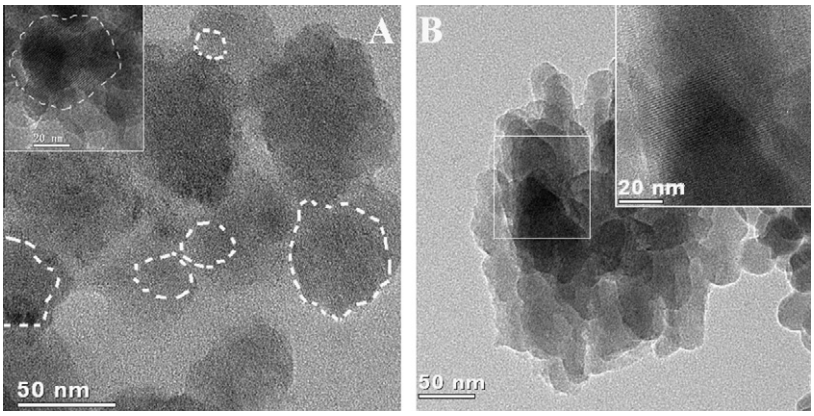

Fig. 4. TEM images of the NZ160-02.

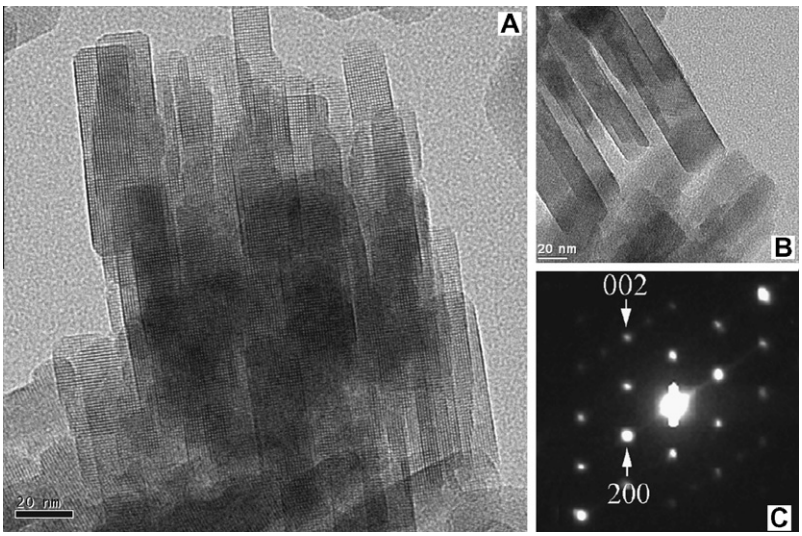

Fig. 5. HRTEM images (A and B) and SAED pattern (C) of NZ160-08.

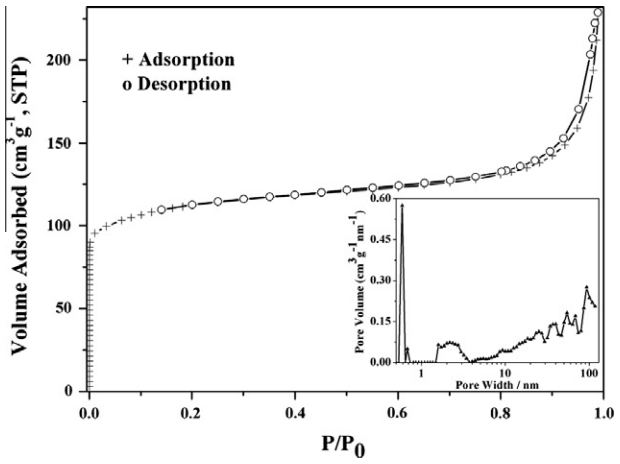

Fig. 6. Nitrogen adsorption/desorption isotherm and DFT pore-size distributions of the single-crystal-like zeolitic architecture (NZ160-08).

continuously increases until a hydrothermal time reaching 8 h. This may be explained by the shrinkage of the average mesopore size accompanying the crystallization process. The NZ160-08 presents the optimized textural properties with its relative large surface area and pore volume for both micro- (246 $m^2 g^{-1}$ and 0.12 $cm^3 g^{-1}$) and mesopores (123 $m^2 g^{-1}$ and 0.17 $cm^3 g^{-1}$), indicating that this sample has been well crystallized and meanwhile retained the enriched supermicro- and mesopores within the particles (Fig. 6). It is very interesting that the mesopores in NZ160-08 could be considered not only as the intercrystalline pores among the oriented zeolite nanorods but also as the intracrystalline pores in the unique monocrystal-like structure, referring to the TEM images (Fig. 5). Compared with NZ160-08, CZ-3 has almost the same surface area and pore volume of the micropore but a lower mesopore volume and external surface area (Table 1).

The silicalite-1 seeds preadded in the synthesis mixtures play a crucial induction role in the formation of hierarchical structured ZSM-5 zeolite. Fig. 7 depicts the XRD pattern and TEM images of the prepared silicalite-1 seeds, respectively. It is found the formed seeds have spontaneously aligned to oriented aggregates from their almost continuous lattice fringes over the adjacent crystallites (Fig. 7B). For the monodispered zeolite particle, the protrusions illustrated by arrowheads are the aggregative silicalite-1 nanoparticles with same orientation (Fig. 7C). It has been regarded as the oriented aggregation mechanism in recent literature [27,28]. When the seeds were added into the synthesis system, they would serve as the initial crystal cores to induce the secondary nucleation and the growth of the nanosized ZSM-5 crystals along their preferred orientation of *c*-axis with the assistant direction of 1,6-hexylenediamine [29]. As a result, a new type of hierarchical porous zeolite was obtained by partial intergrowth of the ZSM-5 nanorods with the same orientation. Such oriented aggregation had been reported as an important, nonclassical crystal growth mechanism for

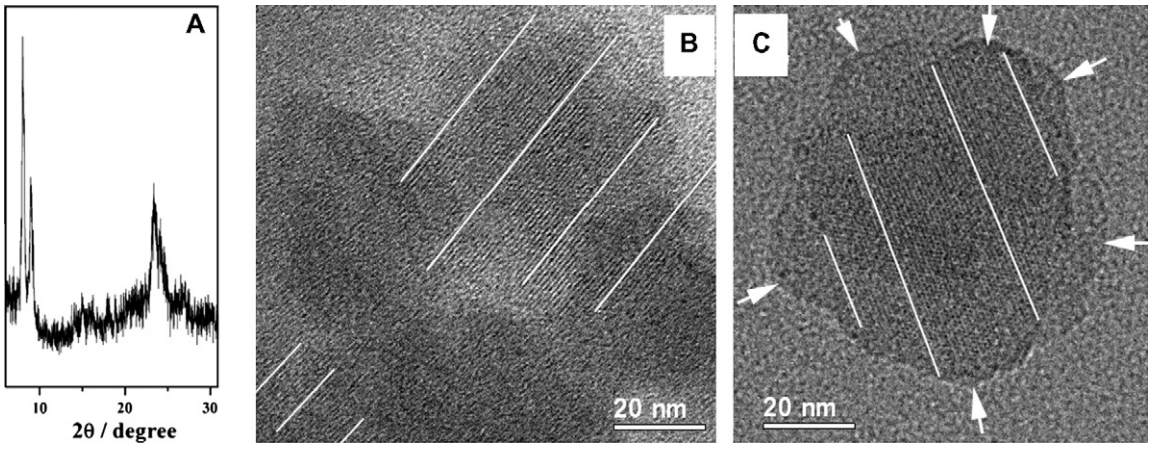

Fig. 7. XRD pattern (A) and TEM images (B and C) of the silicalite-1 seeds.

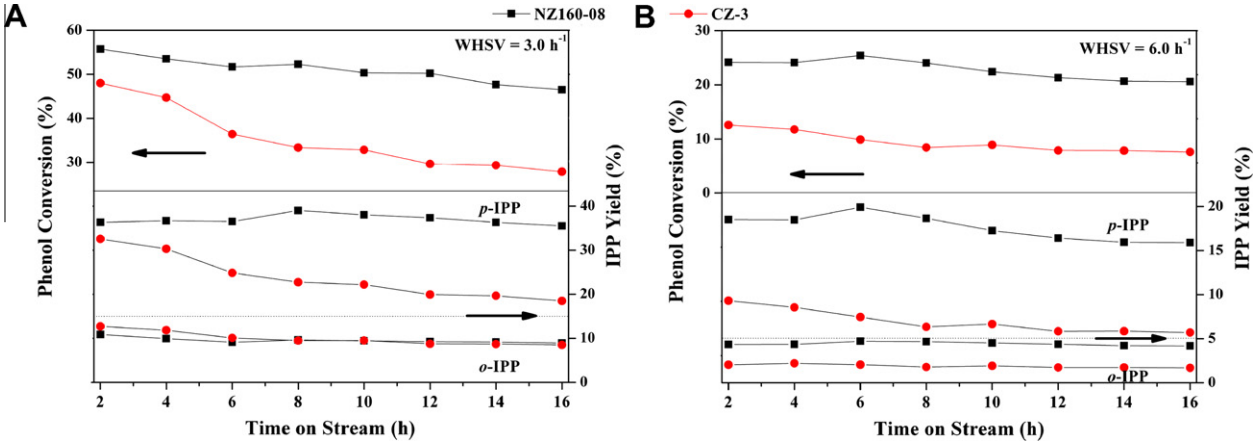

Fig. 8. Catalytic property of NZ160-08 and CZ-3 at WHSV of (A) 3.0 h^{-1} and (B) 6.0 h^{-1}.

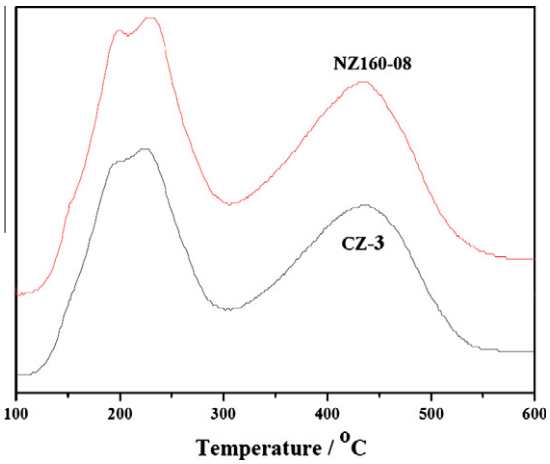

Fig. 9. NH_3-TPD profiles of the protonated NZ160-08 and CZ-3.

the formation of monocrystalline architectures [30–32]. Due to the highly *c*-axis-oriented ZSM-5 zeolite nanocrystal bundle arrays, a novel opening mesopore system was produced as intercrystal pores.

The enhanced opening mesopore volume and large external surface area in the hierarchical porous ZSM-5 zeolite would benefit the reaction and diffusion of the reactant molecules. In this study, the alkylation of phenol with isopropanol (IPA) was used as probe reaction to evaluate the catalytic performance of the protonated NZ160-08 catalyst (Fig. 8). The reaction was carried out in a continuous fixed-bed reactor at 260 °C. The IPA/phenol molar ratio is 1.0 and weight hourly space velocity (WHSV) is 3.0 and 6.0 h^{-1}. The results in Fig. 8 show that NZ160-08 catalyst has both higher phenol conversion and higher yield of *para*-isopropylphenol (*p*-IPP) than CZ-3, although they possess almost the same acidity (Fig. 9). It can be explained by that the ZSM-5 intrinsic micropores can only permit the diffusion and production of *p*-IPP but not *o*-IPP for their space confinement, and the shortened microporous channel and enriched opening mesopores in NZ160-08 will facilitate the production of *p*-IPP, leading to both the high *p*-IPP yield and phenol conversion. Besides, NZ160-08 catalyst also presents a lower deactivation tendency than CZ-3. It could be attributed to the hierarchical structure with enriched micropore openings in NZ160-08, which leads to high coke tolerance.

However, for the yield of *ortho*-isopropylphenol (*o*-IPP), NZ160-08 and CZ-03 show some differences with change of the WHSV. NZ160-08 catalyst has almost the same yield of *o*-IPP as CZ-3 at low WHSV of 3.0 h^{-1} (Fig. 8A) while possessing relatively higher *o*-IPP yield than the latter at high WHSV of 6.0 h^{-1} (Fig. 8B). This is attributed to the synergic effect of the external surface and the diffusion of reactants/products. The partitions of reactants/products in the zeolite intracrystalline volume and those on the external surface should be different for NZ160-08 and CZ-3 due to their different pore structure. At low WHSV, for the short microporous channel and enriched micropore openings, most of reactants would diffuse into the zeolite intracrystalline volume of NZ160-08. Therefore, the reactants distributed on the external surface of NZ160-08 are less than those on the external surface of CZ-03. Accordingly, NZ160-08 and CZ-3 present nearly the same yield of *o*-IPP at WHSV of 3.0 h^{-1} (Fig. 8A), although NZ160-08 has a larger external surface area. As the WHSV is increased to 6.0 h^{-1}, the distribution of reactants on the external surface would be increased for only a certain amount of reaction occurs in intracrystalline active sites. In this case, the large external surface area of NZ160-08 would be beneficial to the reaction for *o*-IPP. As a result, the superiority of a large external surface area of NZ160-08 on the yield of large *o*-IPP becomes distinct (Fig. 8B).

4. Summary

In conclusion, a convenient mesoscale template-free method has been proposed for the preparation of hierarchical structured ZSM-5 zeolite with enriched mesopores as well as large external surface area. The significantly improved catalytic property of the product is due to its easier accessibility of the active sites caused by a shortened microporous channel and opening intercrystal mesopore, which should remarkably extend the zeolite application field.

Acknowledgments

This work was supported by the NSFC (20890122, 20721063), the STCSM (08251203000, 09DZ2271500), 863 program (2009AA033701), and the Major State Basic Research Development Program of China (2009CB623502 and 2009CB623506).

References

[1] D.W. Breck, Zeolite Molecular Sieves, Wiley, New York, 1974.
[2] R.M. Barrer, Hydrothermal Chemistry of Zeolites, Academic Press, London, 1982.
[3] A. Dyer, An Introduction to Zeolite Molecular Sieves, Wiley, Chichester, UK, 1988.
[4] G.A. Ozin, A. Kuperman, A. Stein, Angew. Chem., Int. Ed. Engl. 28 (1989) 359.
[5] S.B. Pu, T. Inui, Zeolites 17 (1996) 334.
[6] J.M. Maselli, A.W. Peters, Catal. Rev. Sci. Eng. 26 (1984) 525.
[7] M.A. Arribas, A. Martinez, Catal. Today 65 (2001) 117.
[8] S. Bernasconi, J.A. van Bokhoven, F. Krumeich, G.D. Pirngrubera, R. Prins, Microporous Mesoporous Mater. 66 (2003) 21.
[9] A.H. Janssen, A.J. Koster, K.P. de Jong, Angew. Chem. Int. Ed. 40 (2001) 1102.
[10] I.I. Ivanova, A.S. Kuznetsov, V.V. Yuschenko, E.E. Knyazeva, Pure Appl. Chem. 76 (2004) 1647.
[11] J.C. Groen, L.A.A. Peffer, J.A. Moulijn, J. Perez-ramirez, Chem. Eur. J. 11 (2005) 4983.
[12] C.J.H. Jacobsen, C. Madsen, J. Houzvicka, I. Schmidt, A. Carlsson, J. Am. Chem. Soc. 122 (2000) 7116.
[13] I. Schmidt, A. Boisen, E. Gustavsson, A.J. Koster, S. Pehrson, S. Dahl, A. Carlsson, C.J.H. Jacobsen, Chem. Mater. 13 (2001) 4416.
[14] Z.X. Yang, Y.D. Xia, R. Mokaya, Adv. Mater. 16 (2004) 727.
[15] Y.M. Fang, H.Q. Hu, J. Am. Chem. Soc. 128 (2006) 10636.
[16] Y.S. Tao, H. Kanoh, K. Kaneko, J. Am. Chem. Soc. 125 (2003) 6044.
[17] F.S. Xiao, L.F. Wang, C.Y. Yin, K.F. Lin, Y. Di, J.X. Li, R.R. Xu, D.S. Su, R. Schlogl, T. Yokoi, T. Tatsumi, Angew. Chem. Int. Ed. 45 (2006) 3090.
[18] M. Choi, H.S. Cho, R. Srivastava, C. Venkatesan, D.-H. Choi, P. Ryoo, Nat. Mater. 5 (2006) 718.
[19] D.P. Serrano, J. Aguado, J.M. Escola, J.M. Rodríguez, Á. Peral, Chem. Mater. 18 (2006) 2462.
[20] R. Srivastava, M. Choi, R. Ryoo, Chem. Commun. (2006) 4489.
[21] M. Choi, R. Srivastava, R. Ryoo, Chem. Commun. (2006) 4380.
[22] R. Krishna, D. Paschek, Phys. Chem. Chem. Phys. 3 (2001) 453.
[23] P. Szabelski, J. Narkiewicz-Michałek, W. Rudzinski, Appl. Surf. Sci. 196 (2002) 191.
[24] S. Nair, M. Tsapatisis, J. Phys. Chem. B 104 (2000) 8982.
[25] C.K. Lee, A.S.T. Chiang, J. Chem. Soc. Faraday Trans. 92 (1996) 3445.
[26] D.J. Wang, Z.N. Liu, Z.K. Xie, J. Inorg. Chem. 23 (2008) 592.
[27] T.M. Davis, T.O. Drews, H. Ramanan, C. He, J.S. Dong, H. Schnablegger, M.A. Katsoulakis, E. Kokkoli, A.V. McCormick, R.L. Penn, M. Tsapatsis, Nat. Mater. 5 (2006) 400.
[28] S. Kumar, T.M. Davis, H. Ramanan, R.L. Penn, M. Tsapatsis, J. Phys. Chem. B 111 (2007) 3398.
[29] C.S. Cundy, P.A. Cox, Microporous Mesoporous Mater. 82 (2005) 1.
[30] R.L. Penn, K. Tanaka, J.J. Erbs, J. Cryst. Growth 309 (2007) 97.
[31] M. Niederberger, H. Cölfen, Phys. Chem. Chem. Phys. 8 (2006) 3271.
[32] Z. Zhang, H. Sun, X. Shao, D. Li, H. Yu, M. Han, Adv. Mater. 17 (2005) 42.